

HYDROGEN-TRIGGERED TYPE I X-RAY BURSTS IN A TWO-ZONE MODEL

RANDALL L. COOPER AND RAMESH NARAYAN

Harvard-Smithsonian Center for Astrophysics, 60 Garden Street, Cambridge, MA 02138

Accepted by THE ASTROPHYSICAL JOURNAL

ABSTRACT

We use the two-zone model of Cooper & Narayan to study the onset and time evolution of hydrogen-triggered type I X-ray bursts on accreting neutron stars. At the lowest accretion rates, thermally unstable hydrogen burning ignites helium as well and produces a mixed hydrogen and helium burst. For somewhat higher accretion rates, thermally unstable hydrogen burning does not ignite helium and thus triggers only a weak hydrogen flash. For our choice of model parameters, these weak hydrogen flashes occur for $10^{-3} \lesssim \dot{M}/\dot{M}_{\text{Edd}} \lesssim 3 \times 10^{-3}$. The peak luminosities of weak hydrogen flashes are typically much lower than the accretion luminosity. These results are in accord with previous theoretical work. We find that a series of weak hydrogen flashes generates a massive layer of helium that eventually ignites in an energetic pure helium flash. Although previously conjectured, this is the first time such bursting behavior has been actually demonstrated in a theoretical model. For yet higher accretion rates, hydrogen burning is thermally stable and thus steadily generates a layer of helium that ultimately ignites in a pure helium flash. We find that, for a narrow range of accretion rates between the mixed hydrogen and helium burst and weak hydrogen flash regimes, unstable hydrogen burning ignites helium only after a short series of weak hydrogen flashes has generated a sufficiently deep layer of helium. These bursts have fluences that are intermediate between those of normal mixed hydrogen and helium bursts and energetic pure helium flashes.

Subject headings: dense matter — nuclear reactions, nucleosynthesis, abundances — stars: neutron — X-rays: binaries — X-rays: bursts

1. INTRODUCTION

Type I X-ray bursts are thermonuclear explosions that occur on the surfaces of accreting neutron stars in low-mass X-ray binaries (Babushkina et al. 1975; Grindlay & Heise 1975; Grindlay et al. 1976; Belian et al. 1976; Woosley & Taam 1976; Joss 1977; Maraschi & Cavaliere 1977; Lamb & Lamb 1977, 1978). They are triggered by unstable hydrogen or helium burning (for reviews, see Lewin et al. 1993, 1995; Cumming 2004; Strohmayer & Bildsten 2006). Theoretical studies of the onset of type I X-ray bursts suggest that there are in general three different bursting regimes separated by accretion rate (Fujimoto et al. 1981; Fushiki & Lamb 1987; Narayan & Heyl 2003). At the highest accretion rates, helium ignites in a hydrogen-rich layer and triggers a mixed hydrogen and helium burst. At somewhat lower accretion rates, nuclear burning via the hot CNO cycle depletes hydrogen before helium ignites, and so thermally unstable helium burning triggers a pure helium flash. At the lowest accretion rates, hydrogen burning itself is thermally unstable (Czerny & Jaroszyński 1980; Ergma & Tutukov 1980).

The vast majority of the type I X-ray bursts that have been observed so far are mixed hydrogen and helium bursts from systems accreting at relatively high rates (van Paradijs et al. 1988; Cornelisse et al. 2003; Remillard et al. 2006; Galloway et al. 2006). This is perhaps to be expected, for the predicted type I X-ray burst rate is in general an increasing function of the accretion rate, and theoretical models predict that the range of accretion rates in which mixed hydrogen and helium bursts occur is rather large. Recently, Galloway & Cumming (2006) observed pure helium bursts from the accretion-powered millisecond pulsar SAX J1808.4–3658 (in 't Zand et al. 1998b). These are the first observed type I X-ray bursts to be unambiguously associated

with the pure helium flash regime. The Wide Field Cameras onboard the *BeppoSAX* satellite observed nine systems that exhibited type I X-ray bursts, but from which no persistent emission was detected (in 't Zand et al. 1998a; Cocchi et al. 1999, 2001; Kaptein et al. 2000; Cornelisse et al. 2002). The lack of persistent emission suggests that these “burst-only” sources have accretion rates $\dot{M} \lesssim 0.01\dot{M}_{\text{Edd}}$, where \dot{M}_{Edd} denotes the mass accretion rate at which the accretion luminosity is equal to the Eddington limit (for a review, see Cornelisse et al. 2004). The low accretion rates imply that the type I X-ray bursts from these sources likely occur in the thermally unstable hydrogen burning regime.

Although it is well understood that hydrogen burning is thermally unstable on neutron stars that accrete at low rates, it is not immediately apparent what will happen after hydrogen ignites. While thermally unstable hydrogen burning will usually ignite helium as well and produce a mixed hydrogen and helium burst, previous investigations have found that there exists a range of accretion rates in which thermally unstable hydrogen burning does not trigger unstable helium burning and therefore produces only a weak hydrogen flash (Ergma & Tutukov 1980; Fujimoto et al. 1981; Fushiki & Lamb 1987; Peng et al. 2007). The low peak X-ray luminosity of the weak hydrogen flashes could possibly render them undetectable. Fushiki & Lamb (1987) and Peng et al. (2007) hypothesize that, within this range of accretion rates, a series of weak hydrogen flashes will produce a sizable layer of nearly pure helium that will eventually trigger an energetic helium flash.

In this investigation, we use a suitably modified version of the two-zone burst model of Cooper & Narayan (2006) to study hydrogen-triggered type I X-ray bursts at low accretion rates. We find that, for a certain range of accretion rates, thermally unstable hydrogen burning does not ignite helium, in

arXiv:astro-ph/0702042v1 1 Feb 2007

agreement with previous investigations. More importantly, we find that, within the aforementioned range of accretion rates, a series of weak hydrogen flashes indeed generates a layer of helium that eventually ignites in an energetic helium flash, thereby confirming the hypothesis of Fushiki & Lamb (1987) and Peng et al. (2007). We begin with a description of the modifications to the two-zone model in §2. We discuss the equilibria of the governing set of differential equations and analyze their stability as a function of accretion rate in §3. In §4 we integrate the governing equations to determine the nature of type I X-ray bursts at different accretion rates. We then summarize our results and conclude in §5.

2. THE MODEL

We assume that matter accretes spherically onto a neutron star of gravitational mass $M = 1.4M_\odot$ and areal radius $R = 10\text{ km}$ at an accretion rate per unit area $\dot{\Sigma}$ as measured in the local frame of the accreted plasma. We consider all physical quantities to be functions of the column depth Σ , which we define as the rest mass of the accreted matter as measured from the stellar surface divided by $4\pi R^2$. We describe the composition of the matter by the hydrogen mass fraction X , helium mass fraction Y , and heavy element fraction $Z = 1 - X - Y$. The mass fractions at $\Sigma = 0$, X_0 , Y_0 , and Z_0 , are those of the accreted plasma. In this work, we assume that all heavy elements are CNO and that the composition of the accreted matter is that of the Sun: $X_0 = 0.7$, $Y_0 = 0.28$, and $Z_0 = 0.02$.

To investigate the stability and time evolution of the accreted plasma, we use the two-zone model of Cooper & Narayan (2006) which consists of (1) a zone that begins at the surface of the star, where $\Sigma = 0$, and extends to the depth Σ_H at which hydrogen is depleted via nuclear burning, and (2) a zone that begins at Σ_H and extends to the depth Σ_{He} at which helium is depleted via nuclear burning. Hydrogen, helium, and CNO are all present in zone 1, while only helium and CNO are present in zone 2. Furthermore, we include both hydrogen and helium burning in zone 1, but we include only helium burning in zone 2. T_H and Z_H denote the temperature and CNO mass fraction at Σ_H , respectively, and T_{He} denotes the temperature at Σ_{He} . For the present study we introduce three modifications to the original two-zone model. (1) For the low accretion rates considered in this work, the temperatures in the accreted layer are often below 8×10^7 K. At these low temperatures, ^{13}N β -decay competes favorably with $^{13}\text{N}(p,\gamma)^{14}\text{O}$, and so hydrogen burns predominantly via the cold CNO cycle (Wiescher et al. 1999) $^{12}\text{C}(p,\gamma)^{13}\text{N}(\beta^+\nu)^{13}\text{C}(p,\gamma)^{14}\text{N}(p,\gamma)^{15}\text{O}(\beta^+\nu)^{15}\text{N}(p,\alpha)^{12}\text{C}$, the rate of which is determined primarily by the slow temperature-dependent reaction $^{14}\text{N}(p,\gamma)^{15}\text{O}$ (Arnould et al. 1992). Therefore, we use the more general prescription for the hydrogen nuclear energy generation rate ϵ_H described in Narayan & Heyl (2003), which includes cold CNO cycle hydrogen burning, with the exceptions that the $^{13}\text{N}(p,\gamma)^{14}\text{O}$ and $^{14}\text{N}(p,\gamma)^{15}\text{O}$ reaction rates are updated to those of Caughlan & Fowler (1988). (2) In this work, the outward heat flux due to non-equilibrium electron captures, neutron emissions, and pycnonuclear reactions that occur in the both the outer and inner crust (Haensel & Zdunik 1990, 2003; Brown 2000; Gupta et al. 2006) largely sets the thermal structure of the accreted layer (Fujimoto et al. 1984; Hanawa & Fujimoto 1984). This is in contrast to the accreted layers on neutron stars that accrete at high rates, for which mixed hydrogen and helium burning sets the

thermal structure. Therefore, we follow Brown (2000) and set the outward flux at the base of the accreted layer due to deep crustal heating $F_{\text{base}} = 0.1\text{ MeV}(\dot{\Sigma}/m_u)$, where m_u is the atomic mass unit. (3) In their derivation of the two differential equations that govern the time evolution of the temperature T_{He} and column depth Σ_{He} of zone 2, the helium-burning zone, Cooper & Narayan (2006) assumed that instantaneous changes of the physical quantities Σ_H , Z_H , and T_H of zone 1 affect the physical quantities Σ_{He} and T_{He} of zone 2. This assumption was physically well-motivated for their work because the thermal and accretion timescales of zone 1 were on the order of the thermal and accretion timescales of zone 2, respectively. As we show in §3, however, the two timescales of zone 2 in this work are much greater than their counterparts in zone 1, so the previously stated assumption is no longer valid. Therefore, we drop this assumption when we derive the differential equations that govern the current model. The result of the new derivation is equivalent to simply omitting the $d\Sigma_H/dt$, dZ_H/dt , and dT_H/dt terms that appear in equations (32) and (33) of Cooper & Narayan (2006). The fundamental equations of our two-zone model are thus

$$\frac{d\Sigma_H}{dt} = 2 \left[\dot{\Sigma} - \frac{\epsilon_H(Z_H, T_H)}{X_0 E_H^*} \Sigma_H \right], \quad (1)$$

$$\frac{dZ_H}{dt} = 2 \frac{\epsilon_{\text{He}}(T_H)}{E_{\text{He}}^*} - \frac{(Z_H - Z_0)}{\Sigma_H} \left(2\dot{\Sigma} - \frac{d\Sigma_H}{dt} \right), \quad (2)$$

$$\frac{dT_H}{dt} = \frac{5}{4C_p} \left[\epsilon_H(Z_H, T_H) + \epsilon_{\text{He}}(T_H) - \frac{F_H - F_{\text{He}}}{\Sigma_H} \right] + \frac{T_H}{4\Sigma_H} \frac{d\Sigma_H}{dt}, \quad (3)$$

$$\frac{d\Sigma_{\text{He}}}{dt} = 2 \left[\dot{\Sigma} - \frac{\epsilon_{\text{He}}(T_{\text{He}})}{(1 - Z_H)E_{\text{He}}^*} \Delta\Sigma \right], \quad (4)$$

$$\begin{aligned} \frac{dT_{\text{He}}}{dt} = & \frac{5(T_{\text{He}}^4 - T_H^4)^2}{4C_p(T_{\text{He}}^8 - 5T_{\text{He}}^4 T_H^4 + 4T_{\text{He}}^3 T_H^5)} \left[\epsilon_{\text{He}}(T_{\text{He}}) - \frac{F_{\text{He}} - F_{\text{base}}}{\Delta\Sigma} \right] \\ & + \frac{T_{\text{He}}}{4\Delta\Sigma} \left[1 - \left(\frac{T_H}{T_{\text{He}}} \right)^4 \right] \frac{d\Sigma_{\text{He}}}{dt} \end{aligned} \quad (5)$$

See Cooper & Narayan (2006) for the definitions of the various symbols.

We emphasize that, in an effort to construct a model that is as simple as possible and yet contains all of the necessary physics needed to describe hydrogen-triggered type I X-ray bursts, we make several assumptions that are not always valid. First, we follow Cooper & Narayan (2006) and assume an ideal gas equation of state, but the electrons are degenerate and set the equation of state at large column depths. In the governing equations (1-5) however, the equation of state of the matter shows up only in the specific heat at constant pressure $C_p = 5k_B/2m_p$. The ion specific heat should dominate that of the electrons for the range of column depths we consider, so our approximation is reasonable. Second, we ignore the density dependence of the helium nuclear energy generation rate ϵ_{He} , and so the rate is somewhat overestimated in zone 1 and underestimated in zone 2. However, considering the other approximations we have made it should be accurate enough for our purposes. Third, we set the opacity to the constant value $\kappa = 0.136\text{ cm}^2\text{ g}^{-1}$. This approximation is probably the most severe. Electron conduction sets the opacity at

the largest column depths we consider in this work, and so the true opacity can be notably smaller than we assume. We discuss the consequences of this approximation in §4.

3. EQUILIBRIA AND THEIR STABILITY

In this section, we solve for the equilibrium solutions of the two-zone model and determine their stability. To find the equilibria, we set $d/dt = 0$, so that equations (1-5) become the following set of five coupled algebraic equations:

$$\epsilon_{\text{H}}(Z_{\text{H}}, T_{\text{H}})\Sigma_{\text{H}} = \dot{\Sigma}X_0E_{\text{H}}^*, \quad (6)$$

$$\epsilon_{\text{He}}(T_{\text{H}})\Sigma_{\text{H}} = \dot{\Sigma}(Z_{\text{H}} - Z_0)E_{\text{He}}^*, \quad (7)$$

$$F_{\text{H}} - F_{\text{He}} = [\epsilon_{\text{H}}(Z_{\text{H}}, T_{\text{H}}) + \epsilon_{\text{He}}(T_{\text{H}})]\Sigma_{\text{H}}, \quad (8)$$

$$\epsilon_{\text{He}}(T_{\text{He}})\Delta\Sigma = \dot{\Sigma}(1 - Z_{\text{H}})E_{\text{He}}^*, \quad (9)$$

$$F_{\text{He}} - F_{\text{base}} = \epsilon_{\text{He}}(T_{\text{He}})\Delta\Sigma. \quad (10)$$

We solve equations (6-10) for the five equilibrium values $\Sigma_{\text{H}}^{\text{eq}}$, Z_{H}^{eq} , T_{H}^{eq} , $\Sigma_{\text{He}}^{\text{eq}}$, and $T_{\text{He}}^{\text{eq}}$. When we do this, we obtain

$$F_{\text{H}}^{\text{eq}} = F_{\text{base}} + \dot{\Sigma} [X_0E_{\text{H}}^* + (1 - Z_0)E_{\text{He}}^*], \quad (11)$$

$$F_{\text{He}}^{\text{eq}} = F_{\text{base}} + \dot{\Sigma}(1 - Z_{\text{H}}^{\text{eq}})E_{\text{He}}^*. \quad (12)$$

Thus the flux emitted from the stellar surface, F_{H}^{eq} , equals the flux released via steady-state nuclear burning of all the fuel plus the flux F_{base} due to deep crustal heating, and the flux entering zone 1, $F_{\text{He}}^{\text{eq}}$, equals the flux released via steady-state nuclear burning of the helium within zone 2 plus that due to deep crustal heating. See Figure 1 for plots of T_{H}^{eq} , $T_{\text{He}}^{\text{eq}}$, $\Sigma_{\text{H}}^{\text{eq}}$, and $\Sigma_{\text{He}}^{\text{eq}}$ as a function of the Eddington-scaled accretion rate

$$l_{\text{acc}} \equiv \frac{\dot{\Sigma}}{\dot{\Sigma}_{\text{Edd}}}, \quad (13)$$

where $\dot{\Sigma}_{\text{Edd}} = 1.0 \times 10^5 \text{ g cm}^{-2} \text{ s}^{-1}$.

The trends seen in Figure 1 may be understood as follows. Hydrogen and helium burning generates energy and heats the accreted layer. In equilibrium, hydrogen and helium burn at a rate $\propto l_{\text{acc}}$, and so the equilibrium temperatures T_{H}^{eq} and $T_{\text{He}}^{\text{eq}}$ are monotonically increasing functions of l_{acc} . For $\log(l_{\text{acc}}) \lesssim -2.5$, the rates at which both hydrogen and helium burn are very temperature-sensitive, and so the depths at which hydrogen and helium deplete, $\Sigma_{\text{H}}^{\text{eq}}$ and $\Sigma_{\text{He}}^{\text{eq}}$, are decreasing functions of l_{acc} . For $T_{\text{H}}^{\text{eq}} \gtrsim 8 \times 10^7 \text{ K}$, however, the proton capture rate onto ^{13}N ($t_{1/2} = 598 \text{ s}$) exceeds that of its β -decay, and so hydrogen burning proceeds via the hot CNO cycle $^{12}\text{C}(p,\gamma)^{13}\text{N}(p,\gamma)^{14}\text{O}(\beta^+\nu)^{14}\text{N}(p,\gamma)^{15}\text{O}(\beta^+\nu)^{15}\text{N}(p,\alpha)^{12}\text{C}$, the rate of which is determined by the slow β -decays of ^{14}O ($t_{1/2} = 70.6 \text{ s}$) and ^{15}O ($t_{1/2} = 122 \text{ s}$) (Hoyle & Fowler 1965). In this case, the hydrogen burning rate depends only on the CNO mass fraction Z_{H} , which is $\approx Z_0$ because $\epsilon_{\text{He}}(T_{\text{H}}^{\text{eq}})/E_{\text{He}}^*$, the rate at which helium burns to carbon, is negligible. Equation (6) thus implies that $\Sigma_{\text{H}}^{\text{eq}} \propto \dot{\Sigma}$. This regime is reflected in the positive slope of $\Sigma_{\text{H}}^{\text{eq}}(l_{\text{acc}})$ in Figure 1.

After we have solved for the equilibrium solution, we conduct a linear stability analysis by assuming that all quantities vary with time as $\exp(\lambda t)$ as described in Cooper & Narayan (2006). The top panel of Figure 2 shows the spectrum of the positive real parts of the eigenvalues λ , and the bottom panel

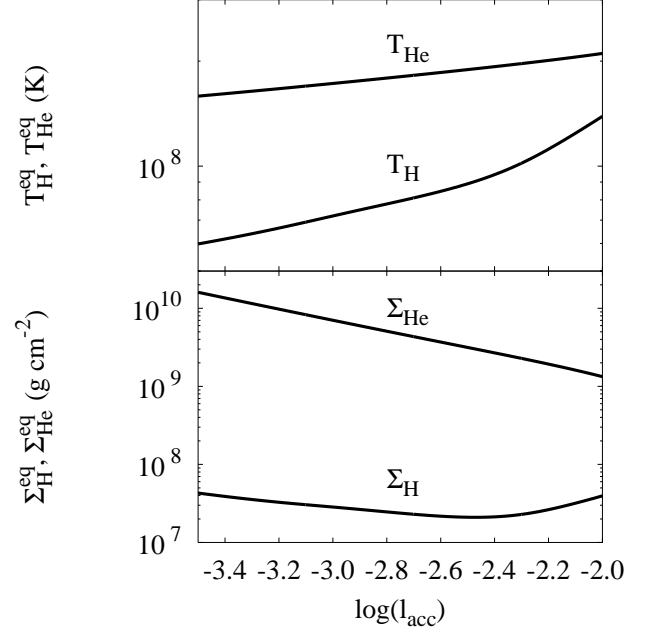


FIG. 1.— Equilibrium values of the four variables T_{H} , T_{He} , Σ_{H} , and Σ_{He} as a function of $l_{\text{acc}} \equiv \dot{\Sigma}/\dot{\Sigma}_{\text{Edd}}$. $Z_{\text{H}}^{\text{eq}} \approx Z_0$ for the entire range of l_{acc} considered in this work. $\Sigma_{\text{H}}^{\text{eq}}$ reaches a local minimum at roughly the same l_{acc} at which T_{H}^{eq} is great enough to initiate hot CNO cycle hydrogen burning.

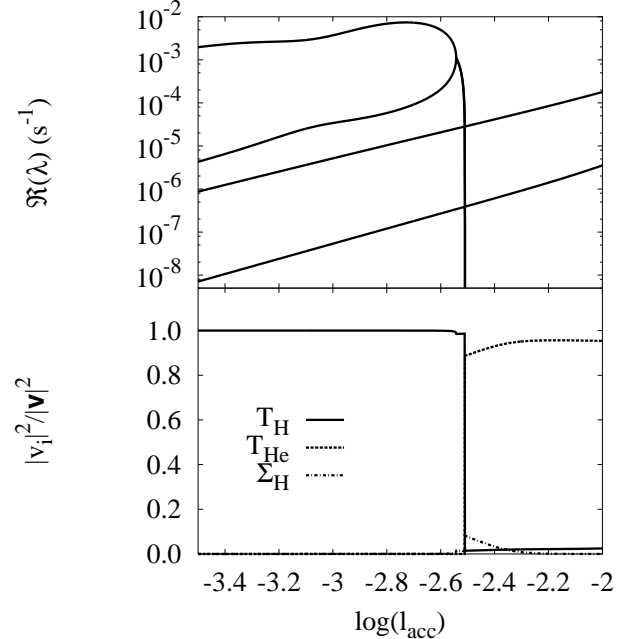


FIG. 2.— Upper panel: real parts of the positive eigenvalues as a function of l_{acc} . Lower panel: normalized components of the eigenvector corresponding to the eigenvalue with the greatest real part. The Z_{H} and Σ_{He} components are negligible and thus are not shown. Both the eigenvalues and eigenvectors show that perturbations in T_{H} trigger bursts for $\log(l_{\text{acc}}) \lesssim -2.5$, and perturbations in T_{He} trigger bursts for $\log(l_{\text{acc}}) \gtrsim -2.5$.

of Figure 2 shows the normalized squared moduli of the components of the eigenvector \mathbf{v} corresponding to the eigenvalue with the greatest real part, both as a function of l_{acc} .

One can ascertain the physical meanings of the eigenvalue spectrum by considering perturbations of proper subsets of

the system of equations (1-5). A linear stability analysis of only equations (1) and (3), which describe perturbations of the hydrogen-burning shell, produces two eigenvalues that are virtually indistinguishable from the two largest eigenvalues of the full system. Similarly, a linear stability analysis of only equations (4) and (5), which describe perturbations of the helium-burning shell, produces two eigenvalues that are virtually indistinguishable from the two lower eigenvalues (which vary nearly linearly with l_{acc} in Figure 2). Thus the two largest eigenvalues that abruptly become negative at $\log(l_{\text{acc}}) \approx -2.5$ describe the stability of hydrogen burning in zone 1, and the other two nearly linear eigenvalues describe the stability of helium burning in zone 2. The clear distinction between the two sets of eigenvalues implies that, according to the linear stability analysis, there is little interaction between zone 1 and zone 2. Physically, this is because $\Sigma_{\text{H}}^{\text{eq}} \ll \Sigma_{\text{He}}^{\text{eq}}$, i.e. the two burning fronts are well-separated. One can deduce this also from the 5×5 Jacobian matrix of the full linear stability analysis. The Jacobian is nearly a block diagonal matrix, with a 3×3 block matrix in the upper left corner that corresponds to the Jacobian of equations (1-3) and a 2×2 block matrix in the lower right corner that corresponds to the Jacobian of equations (4-5). Although the two off-diagonal block matrices are nonzero in general, their matrix elements are negligible relative to those of the two block diagonal matrix elements, which suggests that the full system is reducible to a set of two essentially independent systems.

Only the mode corresponding to the eigenvalue with the greatest real part determines the behavior of the system near the equilibrium (e.g., Guckenheimer & Holmes 1983). From a quick examination of the largest eigenvalue and its corresponding eigenvector shown in Figure 2, our linear stability analysis suggests that thermally unstable hydrogen burning in zone 1 triggers bursts for $\log(l_{\text{acc}}) \lesssim -2.5$ and thermally unstable helium burning in zone 2 triggers bursts for $\log(l_{\text{acc}}) \gtrsim -2.5$. This agrees well with the results of previous theoretical investigations (Fujimoto et al. 1981; Fushiki & Lamb 1987; Narayan & Heyl 2003). Note that the value of l_{acc} at which this transition occurs is in general a decreasing function of $F_{\text{base}}/\dot{\Sigma}$, which is assumed to be $(0.1 \text{ MeV})/m_u$ in this work.

Figure 1 shows that $T_{\text{H}}^{\text{eq}} \gtrsim 8 \times 10^7 \text{ K}$ for $\log(l_{\text{acc}}) \gtrsim -2.5$, and so hydrogen burns via the temperature-independent hot CNO cycle. The hydrogen-burning layer is thus stable to thermal perturbations, and so the eigenvalues corresponding to the hydrogen-burning layer become negative. The thermal eigenvalue of the hydrogen-burning layer passes through zero at approximately the same l_{acc} at which $\Sigma_{\text{H}}^{\text{eq}}$ reaches a local minimum (e.g., Paczyński 1983).

4. NUMERICAL INTEGRATIONS OF THE TWO-ZONE MODEL

The linear stability analyses presented in §3 describe the behavior of the dynamical systems near their respective equilibria. However, the time evolution of a system that is dynamically unstable need not come anywhere close to its equilibrium. This is particularly important for systems in which hydrogen burning is thermally unstable. In this regime, a thermonuclear instability ensues when the column depth of the accreted layer $\Sigma \approx \Sigma_{\text{H}}^{\text{eq}} \ll \Sigma_{\text{He}}^{\text{eq}}$, and so the behavior of Σ_{He} cannot necessarily be deduced from the stability analysis of small perturbations around the equilibrium. Moreover, the linear stability analysis suggests that, in this regime, helium burning in zone 2 is unstable as well, which makes the true time-dependent behavior of the systems especially difficult to predict from the stability analysis alone. In this sec-

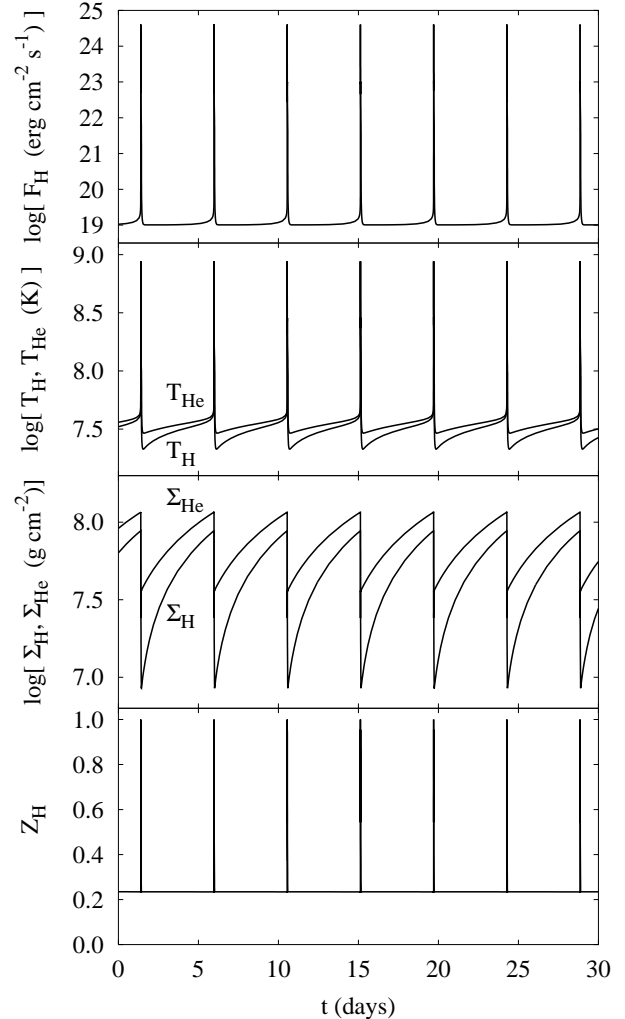


FIG. 3.— Time evolution of type I X-ray bursts for $\log(l_{\text{acc}}) = -3.0$. The top panel shows the light curve, and the bottom three panels show the time evolution of the five physical quantities. Note that $T_{\text{He}} > T_{\text{H}}$ and $\Sigma_{\text{He}} > \Sigma_{\text{H}}$. Sudden drops in both Σ_{H} and Σ_{He} during bursts indicate that both hydrogen and helium have ignited and thus have triggered a mixed hydrogen and helium burst.

tion, we remedy this by numerically integrating equations (1-5) to study the nonlinear development of the instability and the limit cycle behavior of type I X-ray bursts at different accretion rates.

We initiate all numerical integrations by perturbing the equilibrium solution, and we continue the integration until the system reaches a limit cycle. The limit cycle behavior is completely insensitive to the initial conditions. Figure 3 shows the limit cycle behavior for a system with $\log(l_{\text{acc}}) = -3.0$. At the lowest accretion rates we consider in this work, unstable hydrogen burning via the cold CNO cycle raises the temperature of the accreted layer to such an extent as to trigger unstable helium burning as well. The sudden drops in both Σ_{H} and Σ_{He} that correspond with sudden increases in the temperatures T_{H} and T_{He} and the outward flux F_{H} indicate that both hydrogen and helium ignite in every burst. These bursts are the well-known mixed hydrogen and helium type I X-ray bursts triggered by thermally unstable hydrogen burning (Ergma & Tutukov 1980; Fujimoto et al. 1981; Fushiki & Lamb 1987; Peng et al. 2007).

For somewhat higher accretion rates, theory predicts that the increase in temperature due to thermally unstable hydro-

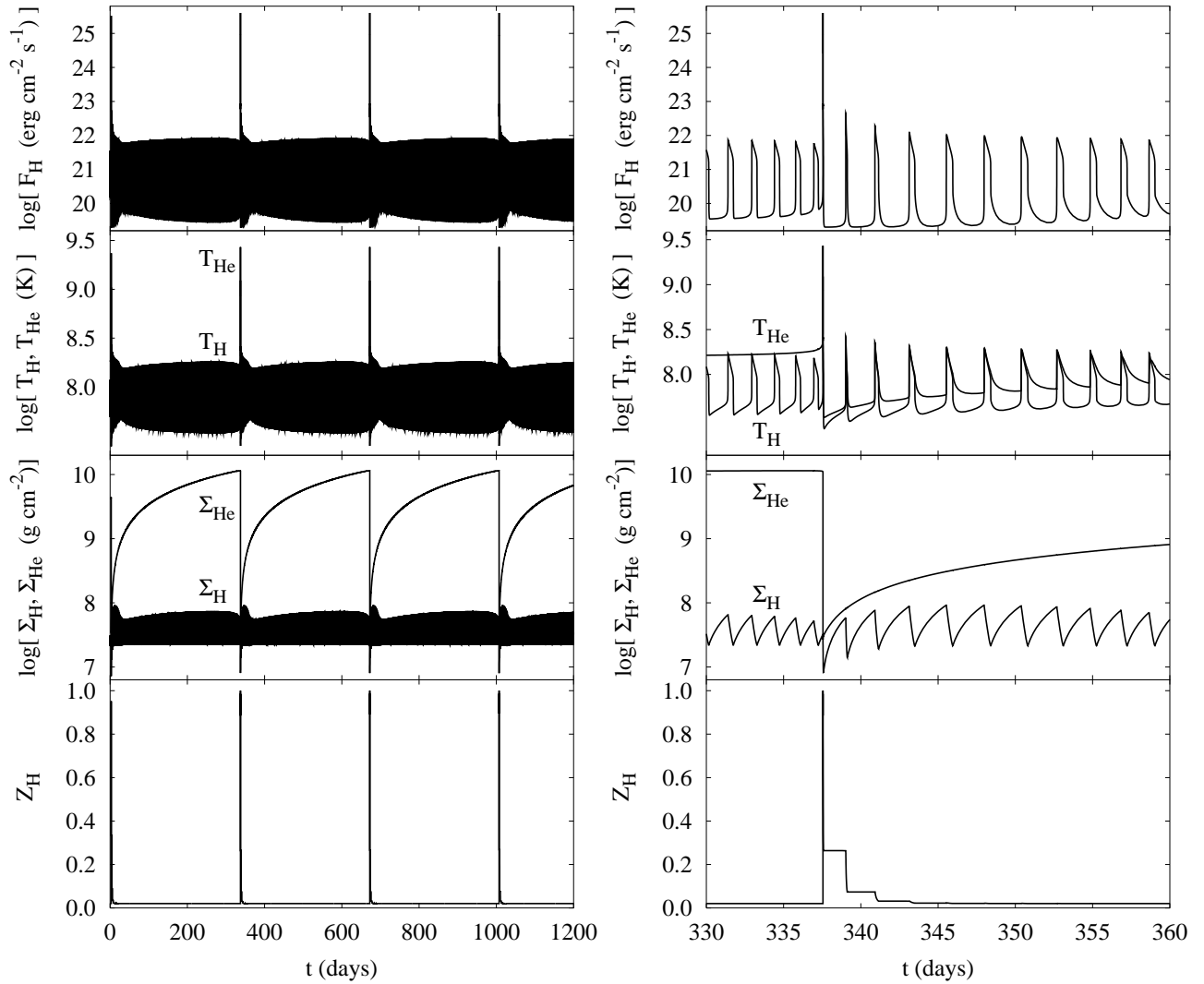


FIG. 4.— Time evolution of bursts for $\log(l_{\text{acc}}) = -2.7$. The top panel on the left shows the light curve, and the bottom three panels show the time evolution of the five physical quantities. Note that $T_{\text{He}} > T_{\text{H}}$ and $\Sigma_{\text{He}} > \Sigma_{\text{H}}$. The increase in T_{H} due to thermally unstable hydrogen burning is insufficient to trigger helium ignition. Therefore, Σ_{He} increases during a long series of weak hydrogen flashes until helium ignites and produces an energetic pure helium flash. The set of panels on the right illustrates the time evolution of the system just before and after an energetic pure helium flash.

gen burning is insufficient to ignite helium. Previous authors have speculated that a series of weak hydrogen flashes allows for the accumulation of a large layer of helium and eventually leads to a strong helium flash (Taam 1981; Fushiki & Lamb 1987; Peng et al. 2007). We present in Figure 4 the results of a calculation for a system with $\log(l_{\text{acc}}) = -2.7$ that confirms this suggestion: if thermally unstable hydrogen burning does not ignite helium, helium will accumulate up to a column depth $\Sigma_{\text{He}} \sim 10^{10} \text{ g cm}^{-2}$ and eventually ignite in an energetic helium flash. Subsequent weak hydrogen flashes ensue until a sufficient amount of helium can accumulate and once again trigger an energetic helium flash. To our knowledge, this is the first study in which this limit cycle behavior has been explicitly demonstrated.

The bursting behavior of systems with accretion rates that lie in a small range between those of the two regimes described above can be somewhat chaotic. Figure 5 shows the light curve F_{H} and the time evolution of the helium column depth Σ_{He} for five different accretion rates that span the transition region between the two aforementioned bursting regimes. As we increase the accretion rate from $\log(l_{\text{acc}}) = -2.93$ to -2.87 , a comparison between F_{H} and Σ_{He} illustrates that the

bursting behavior evolves from that of exclusively mixed hydrogen and helium bursts, to a combination of both mixed bursts and weak hydrogen flashes, to predominantly weak hydrogen flashes with infrequent but unusually energetic mixed bursts. The left panel of Figure 5 shows that the amount of helium fuel burned in the mixed bursts increases with accretion rate. Thus the burst fluences of the mixed bursts in this transition region are intermediate between the mixed bursts at slightly lower l_{acc} and the energetic pure helium bursts and slightly higher l_{acc} .

For $\log(l_{\text{acc}}) \gtrsim -2.5$, Figure 2 implies that hydrogen burning is thermally stable. Consequently, steady-state hydrogen burning generates a sizable column of nearly pure helium as accretion ensues until the helium at the base of the accreted layer ignites. Figure 6 depicts the limit cycle behavior of such a system with $\log(l_{\text{acc}}) = -2.0$. The existence and nature of these pure helium-shell flashes are well-established in theoretical models (Fujimoto et al. 1981; Hanawa & Fujimoto 1982; Fushiki & Lamb 1987; Bildsten 1998; Cumming & Bildsten 2000; Narayan & Heyl 2003; Woosley et al. 2004; Cumming et al. 2006). Note that the column depths Σ_{He} at which helium ignites shown in Figures 4

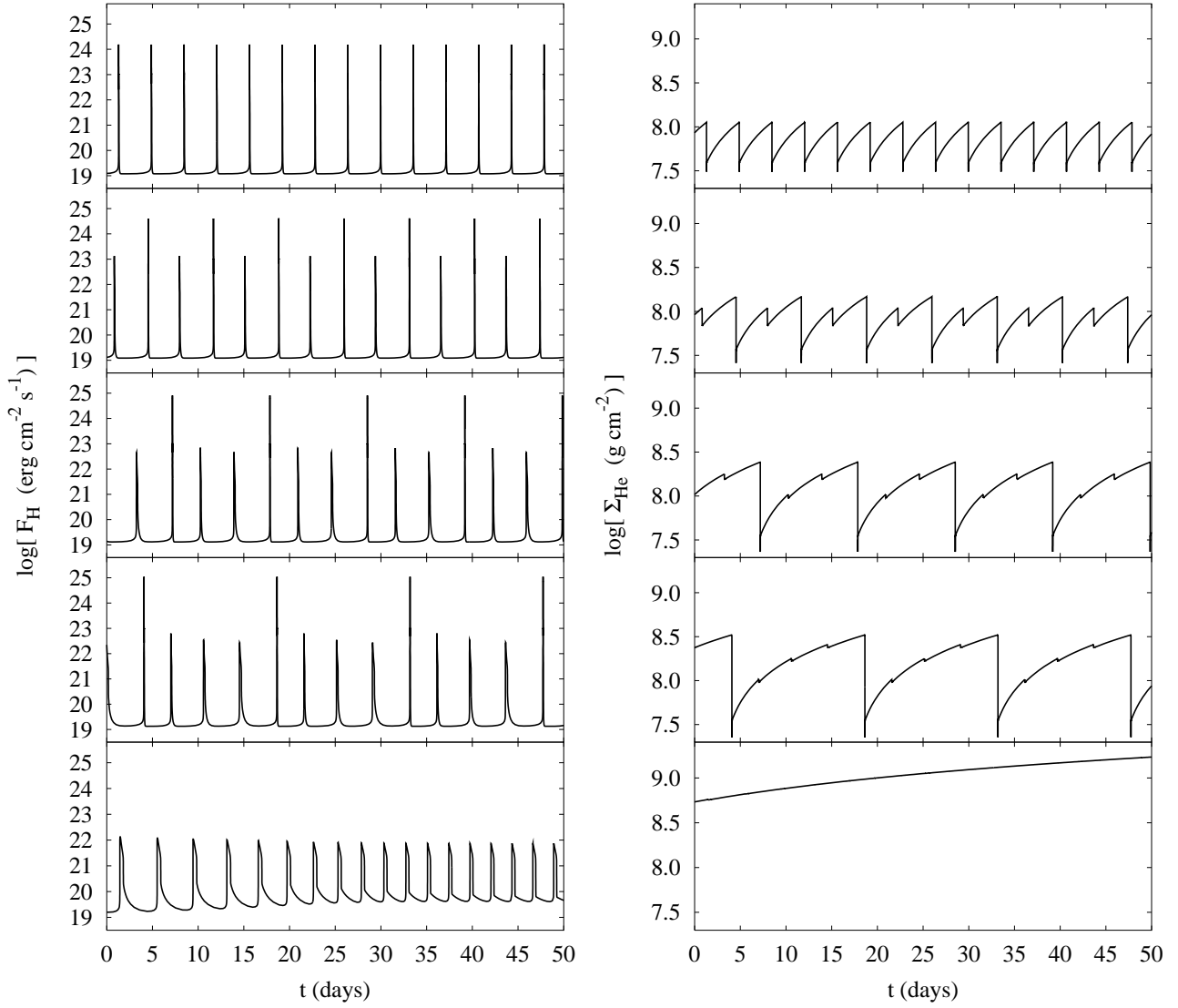


FIG. 5.— Burst light curves (left) and Σ_{He} (right) for $\log(l_{\text{acc}}) = -2.93, -2.92, -2.89, -2.88,$ and -2.87 , from top to bottom. For $\log(l_{\text{acc}}) = -2.93$, the T_{H} increase due to thermally unstable hydrogen burning is always sufficient to ignite all of the helium. For slightly larger values of l_{acc} , unstable hydrogen burning triggers complete helium ignition only if Σ_{He} is sufficiently large, and the ensuing mixed hydrogen and helium bursts are therefore less frequent and more energetic. For $\log(l_{\text{acc}}) = -2.87$, unstable hydrogen burning never ignites helium.

and 6 are generally lower than those found by Cumming et al. (2006) and Peng et al. (2007). This is due to our simplification that the opacity $\kappa = 0.136 \text{ cm}^2 \text{ g}^{-1}$ throughout the entire layer. At these large column depths, electron conduction sets the opacity, and so the true κ is lower than our assumed value. Since the opacity is lower, a larger column of accreted matter must be accreted before helium burning can become thermally unstable.

We plot the recurrence time, burst energy, α -value, and maximum Eddington-scaled flux of type I X-ray bursts as a function of l_{acc} in Figure 7. All quantities are as measured by an observer at infinity. For $-2.9 \lesssim \log(l_{\text{acc}}) \lesssim -2.5$, both energetic pure helium flashes and weak hydrogen flashes occur. In this regime, the solid lines in the four panels denote the burst properties of the helium flashes, and the dot-and-dashed lines denote the burst properties of the hydrogen flashes. The recurrence time is defined as the time between two successive flashes. We calculate the burst energy by determining the total amount of hydrogen and helium fuel that exists just prior to a burst and assuming that all of the fuel burns during a burst.

Since essentially no helium burns during a weak hydrogen flash, however, we determine the burst energy of such a flash by instead assuming that the burst consumes only hydrogen. The parameter α is defined as the accretion energy released between successive bursts divided by the nuclear energy released during a burst. For the range of accretion rates in which both energetic pure helium flashes and weak hydrogen flashes occur, the larger α in Figure 7 is the value an observer would measure if only the energetic helium flashes were detected, and the smaller α is the value an observer would measure if the weak hydrogen flashes were detected as well. Since the peak flux of weak hydrogen flashes is usually much less than the accretion luminosity, as is evident in the bottom panel of Figure 7, it is possible that weak hydrogen flashes would be undetected. Note that, as Figure 4 illustrates, the properties of the weak hydrogen flashes for a given l_{acc} vary somewhat with time. Consequently, the quantities plotted in Figure 7 that describe weak hydrogen bursts are only approximate.

The ranges of accretion rates within which the various bursting regimes lie depend upon the value of the outward

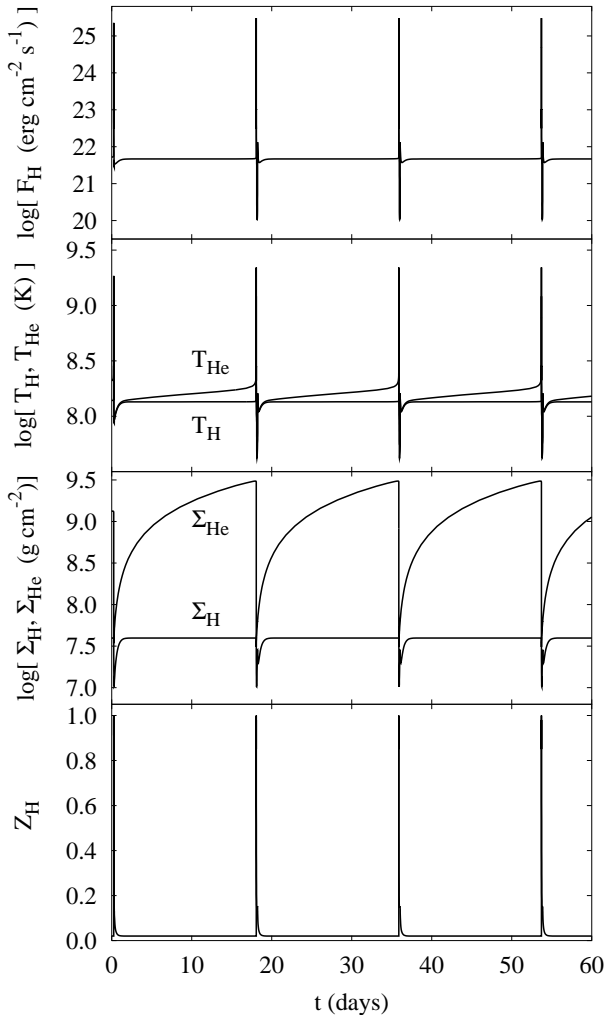


FIG. 6.— Time evolution of bursts for $\log(l_{\text{acc}}) = -2.0$. The top panel shows the light curve, and the bottom three panels show the time evolution of the five physical quantities. $T_{\text{H}} \gtrsim 10^8$ K, so hydrogen burns via the temperature-independent and thus thermally stable hot CNO cycle. Consequently, stable hydrogen burning generates a large and nearly pure helium layer that eventually ignites in an energetic helium flash.

flux at the base of the accreted layer F_{base} , which we set to $0.1 \text{ MeV}(\dot{\Sigma}/m_{\text{u}})$. However, for the low accretion rates we consider in this work, F_{base} may be significantly larger (Brown 2004). When we instead set $F_{\text{base}} = 1.0 \text{ MeV}(\dot{\Sigma}/m_{\text{u}})$, we find that weak hydrogen flashes occur for $-3.95 \lesssim \log(l_{\text{acc}}) \lesssim -2.55$. This range is lower than that shown in Figure 7, and it is qualitatively consistent with the results of Peng et al. (2007).

Our numerical integrations expose a fundamental weakness of linear stability analyses. While one can accurately determine whether or not a system is stable to perturbations using a linear stability analysis, one cannot necessarily infer with any confidence the nature of a system that is unstable. For example, numerical integrations demonstrate that a transition between hydrogen-triggered mixed bursts and weak hydrogen flashes occurs at $\log(l_{\text{acc}}) \approx -2.9$, but neither the eigenvalues nor the eigenvector shown in Figure 2 indicate any change in the physical behavior of the system near this accretion rate. This weakness exists even in the more complete global linear stability analysis of Narayan & Heyl (2003). In that work, the authors found that hydrogen burning is thermally unstable at low accretion rates as well, but again they were unable to de-

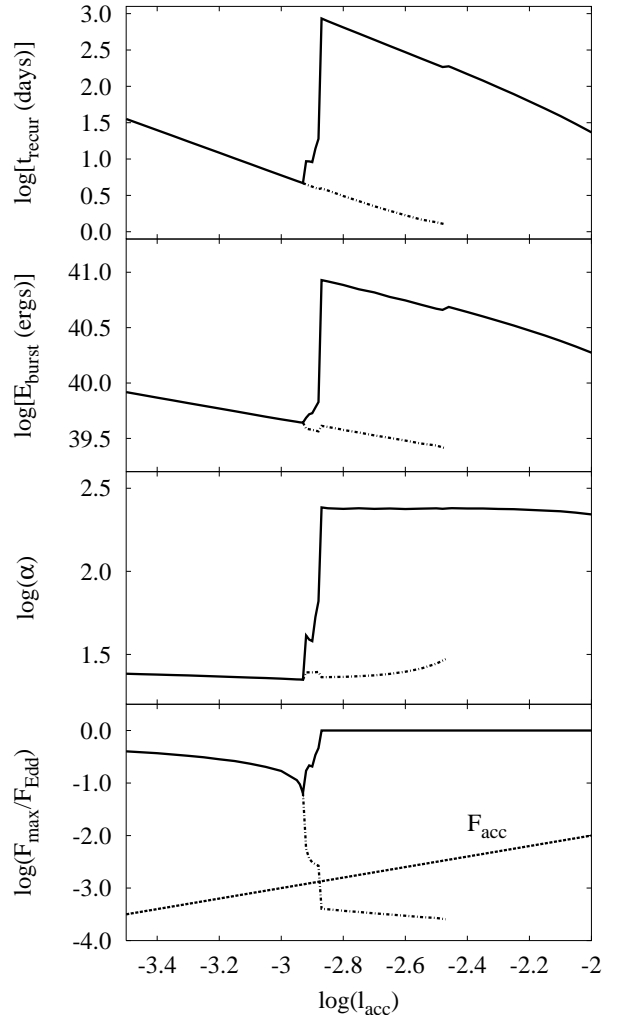


FIG. 7.— Recurrence time, burst energy, ratio of accretion to burst energy α , and peak flux of type I X-ray bursts as a function of l_{acc} , from top to bottom. For $-2.9 \lesssim \log(l_{\text{acc}}) \lesssim -2.5$, both energetic pure helium flashes and weak hydrogen flashes occur. In this case, the solid line denotes the burst properties of the helium flashes and the dot-and-dashed line denotes the burst properties of the hydrogen flashes. The chaotic behavior discussed in §4 and Fig. 5 causes the sudden jumps in the panels that occur in the range $-2.93 < \log(l_{\text{acc}}) < -2.87$. The dashed line in the bottom panel denotes the luminosity due to accretion. Note that the peak flux during most weak hydrogen flashes is much less than the accretion luminosity.

duce the nature of the instability from their results. Thus, one must use caution when inferring the time-dependent behavior of a system that is unstable according to a linear stability analysis.

5. SUMMARY AND CONCLUSIONS

Using a suitably modified version of the two-zone model of Cooper & Narayan (2006), we have studied both the onset and time evolution of hydrogen-triggered type I X-ray bursts on accreting neutron stars. At the lowest accretion rates we have considered, thermally unstable hydrogen burning triggers thermally unstable helium burning and thus produces a mixed hydrogen and helium burst. For somewhat higher accretion rates, thermally unstable hydrogen burning does not ignite helium and thus triggers only a weak hydrogen flash, in agreement with previous studies. For our choice of model parameters, these weak hydrogen flashes occur for $10^{-3} \lesssim \dot{M}/\dot{M}_{\text{Edd}} \lesssim 3 \times 10^{-3}$. We find that, in accord with the predictions of Fushiki & Lamb (1987) and Peng et al. (2007),

subsequent weak hydrogen flashes generate a sizable layer of nearly pure helium that eventually ignites in an energetic pure helium flash. This is the first time this bursting behavior has been seen in theoretical models. For yet higher accretion rates, hydrogen burning is thermally stable and thus steadily generates a layer of helium that ultimately ignites in a pure helium flash. In addition, we find that there exists a small range of accretion rates near the boundary between the mixed hydrogen and helium burst and weak hydrogen flash regimes where thermally unstable hydrogen burning ignites helium only after Σ_{He} is sufficiently large. The resulting mixed hydrogen and helium type I X-ray bursts have fluences that are intermediate between the normal mixed hydrogen and helium bursts and the energetic pure helium flashes.

The simplicity of our two-zone model has enabled us to survey a wide range of accretion rates and to illustrate the basic physics of hydrogen-triggered type I X-ray bursts in the various bursting regimes. However, there are several pieces of physics we have not considered that certainly would affect the nature of type I X-ray bursts at the low accretion rates considered in this work. First, the timescale for sedimentation and diffusion of heavy elements in the accreted layer is often less than the accretion timescale (Wallace et al. 1982; Bildsten et al. 1992; Peng et al. 2007). Peng et al. (2007) demonstrate that the sedimentation of CNO ions can have a notable effect on the ignition conditions of type I X-ray bursts at very low accretion rates. Second, our effective nuclear reaction network consists only of hydrogen burning via the cold and hot CNO cycles and helium burning via the triple- α process. During a mixed hydrogen and helium burst, however, hydrogen will burn predominantly via the *rp*-process of Wallace & Woosley (1981). Consequently, the light curves of these bursts would be somewhat different than those shown in

Figure 3 if *rp*-process hydrogen burning were included.

A potentially serious issue that we are currently unable to address, but that could have significant effects on the ignition of type I X-ray bursts at low accretion rates, is the destruction of CNO ions via nuclear spallation reactions (Bildsten et al. 1992). The accretion disks around neutron stars that accrete at low rates are likely truncated (e.g. Done 2002; Barret 2004). Within the truncated disk, the accretion flow is optically thin and quasi-spherical (see, e.g. Narayan & Yi 1995), and thus the accreting ions have large radial velocities when they reach the neutron star surface. Observationally, this radiatively inefficient accretion flow occurs in neutron star low-mass X-ray binaries when $\dot{M} \lesssim 0.01\dot{M}_{\text{Edd}}$ (Mendez et al. 1997; Gierliński & Done 2002), the range of accretion rates applicable to this work. The directed kinetic energy of the accreting hydrogen and helium may be sufficient to destroy nearly all of the ions in the envelope that are heavier than helium. The degree to which spallation would affect type I X-ray burst ignition is unclear. Compositional inertia of the neutron star envelope could potentially counteract any depletion of CNO due to spallation (Ayasli & Joss 1982; Woosley & Weaver 1984; Taam et al. 1993; Woosley et al. 2004). However, if the heavy elements produced in a given burst sediment out of the envelope before the next burst is triggered, compositional inertia may be negligible, in which case spallation again becomes important. This issue in particular is worthy of further investigation.

We would like to thank Edward Brown, Andrew Cumming, and Fang Peng for useful discussions and the referee for several comments that helped us improve this investigation. This work was supported by NASA grant NNG04GL38G.

REFERENCES

- Arnould, M., Paulus, G., & Jorissen, A. 1992, *A&A*, 254, L9
 Ayasli, S. & Joss, P. C. 1982, *ApJ*, 256, 637
 Babushkina, O. P., Bratolyubova-Tsulukidze, L. S., Kudryavtsev, M. I., Melioranskiy, A. S., Savenko, I. A., & Yushkov, B. Y. 1975, *Soviet Astronomy Letters*, 1, 32
 Barret, D. 2004, in *AIP Conf. Proc. 703: Plasmas in the Laboratory and in the Universe: New Insights and New Challenges*, ed. G. Bertin, D. Farina, & R. Pozzoli, 238–249
 Belian, R. D., Conner, J. P., & Evans, W. D. 1976, *ApJ*, 206, L135
 Bildsten, L. 1998, in *NATO ASIC Proc. 515: The Many Faces of Neutron Stars*, 419
 Bildsten, L., Salpeter, E. E., & Wasserman, I. 1992, *ApJ*, 384, 143
 Brown, E. F. 2000, *ApJ*, 531, 988
 Brown, E. F. 2004, *ApJ*, 614, L57
 Caughlan, G. R. & Fowler, W. A. 1988, *Atomic Data and Nuclear Data Tables*, 40, 283
 Cocchi, M., Bazzano, A., Natalucci, L., Ubertini, P., Heise, J., Kuulkers, E., Cornelisse, R., & in 't Zand, J. J. M. 2001, *A&A*, 378, L37
 Cocchi, M., Bazzano, A., Natalucci, L., Ubertini, P., Heise, J., Muller, J. M., & in 't Zand, J. J. M. 1999, *A&A*, 346, L45
 Cooper, R. L. & Narayan, R. 2006, *ApJ*, 652, 584
 Cornelisse, R., in 't Zand, J. J. M., Kuulkers, E., Heise, J., Verbunt, F., Cocchi, M., Bazzano, A., Natalucci, L., & Ubertini, P. 2004, *Nuclear Physics B Proceedings Supplements*, 132, 518
 Cornelisse, R., in 't Zand, J. J. M., Verbunt, F., Kuulkers, E., Heise, J., den Hartog, P. R., Cocchi, M., Natalucci, L., Bazzano, A., & Ubertini, P. 2003, *A&A*, 405, 1033
 Cornelisse, R., Verbunt, F., in 't Zand, J. J. M., Kuulkers, E., Heise, J., Remillard, R. A., Cocchi, M., Natalucci, L., Bazzano, A., & Ubertini, P. 2002, *A&A*, 392, 885
 Cumming, A. 2004, *Nuclear Physics B Proceedings Supplements*, 132, 435
 Cumming, A. & Bildsten, L. 2000, *ApJ*, 544, 453
 Cumming, A., Macbeth, J., in 't Zand, J. J. M., & Page, D. 2006, *ApJ*, 646, 429
 Czerny, M. & Jaroszyński, M. 1980, *Acta Astronomica*, 30, 157
 Done, C. 2002, *Royal Society of London Philosophical Transactions Series A*, 360, 1967
 Ergma, E. V. & Tutukov, A. V. 1980, *A&A*, 84, 123
 Fujimoto, M. Y., Hanawa, T., Iben, Jr., I., & Richardson, M. B. 1984, *ApJ*, 278, 813
 Fujimoto, M. Y., Hanawa, T., & Miyaji, S. 1981, *ApJ*, 247, 267
 Fushiki, I. & Lamb, D. Q. 1987, *ApJ*, 323, L55
 Galloway, D. K., & Cumming, A. 2006, *ApJ*, 652, 559
 Galloway, D. K., Muno, M. P., Hartman, J. M., Savov, P., Psaltis, D., & Chakrabarty, D. 2006, *ApJS*, submitted (astro-ph/0608259)
 Gierliński, M. & Done, C. 2002, *MNRAS*, 337, 1373
 Grindlay, J., Gursky, H., Schnopper, H., Parsignault, D. R., Heise, J., Brinkman, A. C., & Schrijver, J. 1976, *ApJ*, 205, L127
 Grindlay, J. & Heise, J. 1975, *IAU Circ.*, 2879
 Guckenheimer, J. & Holmes, P. 1983, *Nonlinear Oscillations, Dynamical Systems, and Bifurcations of Vector Fields (Applied Mathematical Sciences, New York: Springer)*
 Gupta, S., Brown, E. F., Schatz, H., Moeller, P., & Kratz, K.-L. 2006, *ApJ*, submitted (astro-ph/0609828)
 Haensel, P. & Zdenek, J. L. 1990, *A&A*, 227, 431
 —. 2003, *A&A*, 404, L33
 Hanawa, T. & Fujimoto, M. Y. 1982, *PASJ*, 34, 495
 —. 1984, *PASJ*, 36, 199
 Hoyle, F. & Fowler, W. A. 1965, in *Quasi-Stellar Sources and Gravitational Collapse*, 17
 in 't Zand, J. J. M., Heise, J., Muller, J. M., Bazzano, A., Cocchi, M., Natalucci, L., & Ubertini, P. 1998a, *Nuclear Physics B Proceedings Supplements*, 69, 228
 —. 1998b, *A&A*, 331, L25
 Joss, P. C. 1977, *Nature*, 270, 310
 Kaptein, R. G., in 't Zand, J. J. M., Kuulkers, E., Verbunt, F., Heise, J., & Cornelisse, R. 2000, *A&A*, 358, L71

- Lamb, D. Q. & Lamb, F. K. 1977, in *Eight Texas Symposium on Relativistic Astrophysics*, ed. M. D. Papagiannis (New York: New York Academy of Sciences), 261
- Lamb, D. Q. & Lamb, F. K. 1978, *ApJ*, 220, 291
- Lewin, W. H. G., van Paradijs, J., & Taam, R. E. 1993, *Space Science Reviews*, 62, 223
- . 1995, in *X-ray Binaries*, ed. W. H. G. Lewin et al. (Cambridge: Cambridge Univ. Press)
- Maraschi, L. & Cavaliere, A. 1977, *Highlights of Astronomy*, 4, 127
- Mendez, M., van der Klis, M., van Paradijs, J., Lewin, W. H. G., Lamb, F. K., Vaughan, B. A., Kuulkers, E., & Psaltis, D. 1997, *ApJ*, 485, L37
- Narayan, R. & Heyl, J. S. 2003, *ApJ*, 599, 419
- Narayan, R. & Yi, I. 1995, *ApJ*, 452, 710
- Paczynski, B. 1983, *ApJ*, 264, 282
- Peng, F., Brown, E. F., & Truran, J. W. 2007, *ApJ*, 654, 1022
- Remillard, R. A., Lin, D., Cooper, R. L., & Narayan, R. 2006, *ApJ*, 646, 407
- Strohmayer, T. & Bildsten, L. 2006, in *Compact Stellar X-Ray Sources*, ed. W. H. G. Lewin and M. van der Klis (Cambridge: Cambridge Univ. Press), 113
- Taam, R. E. 1981, *Ap&SS*, 77, 257
- Taam, R. E., Woosley, S. E., Weaver, T. A., & Lamb, D. Q. 1993, *ApJ*, 413, 324
- van Paradijs, J., Penninx, W., & Lewin, W. H. G. 1988, *MNRAS*, 233, 437
- Wallace, R. K. & Woosley, S. E. 1981, *ApJS*, 45, 389
- Wallace, R. K., Woosley, S. E., & Weaver, T. A. 1982, *ApJ*, 258, 696
- Wiescher, M., Görres, J., & Schatz, H. 1999, *Journal of Physics G Nuclear Physics*, 25, 133
- Woosley, S. E., Heger, A., Cumming, A., Hoffman, R. D., Pruet, J., Rauscher, T., Fisker, J. L., Schatz, H., Brown, B. A., & Wiescher, M. 2004, *ApJS*, 151, 75
- Woosley, S. E. & Taam, R. E. 1976, *Nature*, 263, 101
- Woosley, S. E. & Weaver, T. A. 1984, in *AIP Conf. Proc. 115, High Energy Transients in Astrophysics*, ed. S. E. Woosley (New York: AIP), 273